Neurobiology of Disease 218 (2026) 107207

Contents lists available at ScienceDirect

Neurobiology of Disease

journal homepage: www.elsevier.com/locate/ynbdi

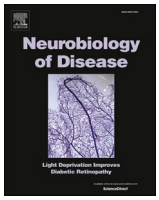

JNK-regulated phosphoproteome links synaptic and metabolic pathways to mood regulation☆

Ye Hong [a,1], Valentina Siino [b,1], Dani Flinkman [a,1], Prasannakumar Deshpande [a], Sylvia Ortega Martinez [a], Veronica Fagerholm [a], Artemis Varidaki [a], Pierre Heemeryck [a], Christel Sourander [a], Peter James [a,b], Eleanor Coffey [a,*]

[a] Turku Bioscience Centre, University of Turku and Åbo Akademi University, Turku 20520, Finland
[b] Department of Immuntechnology, Scheelevägen 2, Medicon Village, House 406, Lund University, Sweden

A B S T R A C T

c-Jun N-terminal kinases (JNKs) are implicated in both neurodegeneration and mood regulation, including anxiety and depressive-like behaviours. Yet the consequences of JNK inhibition in vivo on protein phosphorylation in the brain remain largely unknown. This study aimed to (1) determine how chronic JNK inhibition altered proteome-wide phosphorylation in hippocampus and nucleus accumbens, regions central to affective processing, and (2) determine which JNK-regulated phosphoproteins were associated with the anxiolytic response, representing potential drivers. Mice underwent intracerebral (ICV) infusion with DJNKI-1 or control TAT peptide for six weeks, after which behaviours were assessed and phosphoproteomic profiling performed. JNK inhibition reduced anxiety-like behaviour and significantly altered 163 and 97 phosphosites in the hippocampus and nucleus accumbens, respectively. JNK-regulated phosphoproteins were enriched for regulators of cytoskeleton organization and synaptic function. GSK3 signalling was inhibited by DJNKI-1, leading to extensive depletion of phosphorylation on GSK3 motifs within the hippocampus and nucleus accumbens. These affected proteins involved in adhesion, cytoskeleton, proteostasis and synaptic activity. Moreover, several energy metabolism proteins exhibited phosphorylation changes on sites that control their enzymatic activity. The predicted net effect is a metabolic shift from oxidative phosphorylation to anaerobic glycolysis. Network analysis revealed enhanced phosphoproteome connectivity in mice displaying low anxiety-like behaviour, with spectrin-α/β, syntaxin-1b, CRMP2 and MAPT emerging as central hubs. Notably, claudin-11, an oligodendrocyte-specific, tight junction protein, was identified as a novel phospho-target that was highly reduced upon DJNKI-1 treatment. Together, these findings highlight potential molecular markers of anxiolytic response and suggest synaptic and metabolic interplay in mood regulation.

1. Introduction

c-Jun N-terminal kinases (JNKs) are stress-activated protein kinases that respond to diverse stimuli, including cytokines, endocrine signals, mechanical stress, and ribotoxic insults. Once activated, JNKs phosphorylate target proteins that regulate diverse cellular processes, including autophagy, microtubule stabilization, intracellular transport, insulin signalling, inflammation, and pathways associated with neurodegeneration (Antoniou et al., 2011; Chang et al., 2003; Fu and Holzbaur, 2013; Hotamisligil and Davis, 2016; Hsu et al., 2010; Iordanov et al., 1997; Karpac et al., 2009; Kyriakis and Avruch, 2012; Morfini et al., 2009; Pereira et al., 2011; Vind, 2024; Xu et al., 2011; Zeng et al., 2022). In the nervous system, JNKs are key regulators of neuronal death in models of stroke, Alzheimer's, Parkinson's and Huntington's disease, and JNK inhibitors have been shown to be broadly neuroprotective (Antoniou et al., 2011; Gehringer et al., 2015; Kumari et al., 2023; Peng and Andersen, 2003; Repici and Borsello, 2006; Solas et al., 2023). Despite these important functions, the full spectrum of JNK targets remains poorly characterized. In the brain in particular, the JNK-regulated phosphoproteome is largely unexplored.

JNKs are also implicated in anxiety- and depressive-like behaviours in animal models. Thus, inhibition or genetic deletion of *Jnk1* (*Mapk8*) induces a low-anxiety, low-depressive-like phenotype in rodents (Hollos et al., 2018; Mohammad et al., 2018; Zhao et al., 2017; Zhou et al., 2023). Similarly in zebrafish, JNK inhibitors recapitulate the behavioural phenotype of clinically used antidepressant drugs (Hong et al., 2024). The anxiolytic phenotype evoked by JNK inhibition is associated with increased hippocampal neurogenesis (Castro-Torres et al., 2021; Mohammad et al., 2018), however the underlying phosphorylation changes are unknown. Candidate effectors include cytoskeletal

☆ This article is part of a Special issue entitled: 'Mass Spectrometry and neurological diseases' published in Neurobiology of Disease.

* Corresponding author.
E-mail address: ecoffey@abo.fi (E. Coffey).

[1] Equal contribution.

https://doi.org/10.1016/j.nbd.2025.107207
Received 6 February 2025; Received in revised form 20 November 2025; Accepted 28 November 2025
Available online 29 November 2025
0969-9961/© 2025 The Authors. Published by Elsevier Inc. This is an open access article under the CC BY license (http://creativecommons.org/licenses/by/4.0/).

regulatory protein targets of JNKs, especially those associated with the microtubule cytoskeleton, many of which are also deregulated in psychiatric disorders (Marchisella, 2016).

Here, we analyse the proteome-wide effect of JNK inhibition in the brain, using a well-characterized peptide inhibitor of JNK, DJNKI-1 (Borsello and Bonny, 2004; Borsello et al., 2003). Our results provide the first comprehensive, region-specific phosphoproteomic analysis of chronic JNK inhibition in the mouse hippocampus and nucleus accumbens. Combining phosphoproteomic profiles with behavioural outcomes, reveals specific phosphorylation changes that characterize mice exhibiting an anxiolytic response.

2. Material and methods

2.1. Chronic intracerebroventricular infusion

This procedure was carried out as previously described (Mohammad et al., 2018). For analgesia, adult C57Bl/6 J mice (2-month-old) were injected intraperitoneally with 0.1 mg kg^{-1} of buprenorphine hydrochloride (Reckitt Benckiser Pharmaceuticals, Basel, Switzerland) and anesthetized with 4 % isoflurane and maintained with 2.5 % isoflurane. Local anaesthetic (0.1 ml of 1 mg per 1 μg lidocaine) was subcutaneously injected, before cutting the scalp. A 100 μl mini-osmotic pump (Alzet Model 2006, Cupertino, CA, USA) was inserted subcutaneously at the back of the neck and attached to a cannula that was implanted intracerebroventricularly. Mini-osmotic pumps infused DJNKI-1 or TAT (100 μM) at a rate of 0.15 μl h^{-1}. After 6 weeks, mice underwent behavioural testing. DJNKI-1 peptide inhibitor of JNK was synthesized by Gene Cust, Custom Service for Research (Laboratoire de Biotechnologie du Luxembourg, Dudelange, Luxembourg).

2.2. Behavioural tests

Mice (14 wk. old) were maintained on a 12 h light/dark cycle and supplied with food and water ad libitum. Behavioural tests were conducted between 8 am and 3 pm in the order described with a 2-day interval between tests. The experimenter was blind to the treatment. *Elevated plus maze* - Unconditioned anxiety-like behaviour was monitored using an elevated plus maze (EPM) with two closed (35 × 5 × 15 cm) and two open (35 × 5 cm) arms made of opaque grey plastic elevated at a height of 50 cm above the floor. Mice were placed in the centre of the maze facing a closed arm and allowed to explore freely for 5 min. Behaviour was recorded using the Ethovision video tracking system (Noldus Information Technology, Wageningen, The Netherlands). Automated tracking was used to analyse time spent in the open and closed arms. *Light/dark* - test was performed using a box (30 × 45 × 30 cm), partitioned equally, with opaque black plastic walls with a roof (dark arena) and white walls without roof (light arena) and an opening (5.5 × 7 cm) between partitions. To initiate the test, mice were positioned in the light arena and monitored for 10 min. Time spent in the light and dark area was using video tracking with Ethovision software. Two group comparisons were done using Student's *t*-test.

2.3. Tissue dissection

Two-month old mice underwent cervical dislocation following behavioural tests. The brain was rapidly removed from the skull and transferred to a petri dish containing ice cold PBS, pH 7.4 on ice. Brains were sectioned coronally using an adult mouse brain slicer (Zivic Instruments) at 2.7 and at −4.6 mm from Bregma. NAc (approximately 10 mg) was dissected from the second rostral slice, and the hippocampus from the third. NAc was isolated with inner diameter of 2.0 mm from Bregma 1.54 mm to Bregma 1.04 mm, including both core and shell regions. Afterwards, the third rostral slice was cut by the midline to separate both hemispheres. Hippocampi from each hemisphere, visually recognizable, were isolated. Samples were immediately frozen in liquid nitrogen and stored at −80 °C until homogenization within 3 min of sacrifice.

2.4. Immunohistochemistry

Wild type C57Bl/6 J and *Jnk1*−/− mice at 8 to 12 weeks and originating from the same genetic background were anesthetized with pentobarbital (Mebunat vet, Orion Pharma, Finland) and transcardialy perfused with 4 % paraformaldehyde in phosphate buffered saline (PBS), pH 7.4. Brains were dissected and postfixed in the same solution overnight and then transferred to 20 % sucrose in PBS for one day. Thereafter, brains were frozen by immersion in isopentane chilled with CO_2 ice. Brain sections, 14 μm thick, were prepared using a Leica CM1950 cryostat (Leica Biosystems, Germany) and mounted onto microscope slides (Superfrost Ultra Plus, Menzel-Gläser, Hungary). Slides were dried overnight and stored frozen. After thawing, brain sections were rehydrated in PBS for 10 min. Heat induced antigen retrieval was performed in 10 mM sodium citrate +0.05 % Tween 20, pH 6.0 for 15 min at approximately 100 °C. After rinsing with PBS, slides were incubated in 70 % ethanol for 30 min followed by 3 % H_2O_2 + 10 % methanol for 30 min. After a quick rinse with PBS, slides were incubated in blocking solution (1 % bovine serum albumin +0.4 % Triton X-100 in PBS) for 1 h. Primary antibody (mouse anti-human JNK1 IgG1, clone G151–333, BD Biosciences) was applied at a concentration of 1:15000 in blocking solution for three days at 4 °C. After rinsing in PBS, the slides were incubated with secondary antibody (biotinylated anti-mouse IgG, BA-9200, Vector Laboratories, CA, USA) at a concentration of 1:1000 in blocking solution for 1 h. After rinsing in PBS, the slides were incubated with streptavidin-horseradish peroxidase conjugate (S911, Invitrogen Molecular Probes, OR, USA) at a concentration of 1:2000 in blocking solution for 1 h. After rinsing in PBS, the chromogenic signal was developed for 5 min using DAB (Dako Liquid DAB+ Substrate Chromogen System, Dako K3468, Agilent, CA, USA). The slides were rinsed 2 × 2 min in ultrapure water and were then dehydrated in ethanol, cleared in xylene, and cover-slipped. Representative images of wild type and *Jnk1*−/− brain sections were prepared with a Zeiss AxioVert 200 M microscope and the Zeiss AxioVision software (Carl Zeiss, Germany). Staining was evaluated in both male and female mice. No difference was observed.

2.5. Primary cortical tissue culture

Sprague Dawley rats (P0) were decapitated and cortices dissected in dissociated medium containing kynurenic acid in order to prevent activation of AMPA and NMDA receptors. Mechanical dissociation was performed by pipetting after treatment with papain (100 U) (Worthington) and followed by incubation with trypsin inhibitor (10 mg/ml) (Sigma) to block papain activity. Cells were cultured on surfaces coated with poly-D-Lysine (50 μg/ml). Neurons were grown in MEM medium supplemented with 10 % Fetal Bovine Serum, 30 mM Glucose, 2 mM Glutamine and Penicillin (50 U/ml)/Streptomycin (50 μg/ml) at a density of 2700 cells/mm^2. After 48 h, 2.5 μM cytosine arabinofuranoside (Sigma, St. Louis, MO) was added to the cultures and cells were maintained in a humidified incubator with 5 % CO_2 at 37 °C.

2.6. Cell treatment

Cortical neurons at 16 days in vitro were treated with 20 μM TAT or DJNKI-1 peptide (Gene Cust, Custom Services for Research, Laboratoire de Biotechnologie du Luxembourg, Dudelange, Luxemburg) for the times indicated. Cells were lysed in 1× *Laemmli* buffer followed by boiling for 5 min.

2.7. Immunoblotting

Lysates were subjected to sodium dodecyl sulfate (SDS)-

polyacrylamide gel electrophoresis. Protein transfer was performed using nitrocellulose membranes. Membranes were incubated with 1× TBS-T (TBS containing 0.1 % Tween-20) and 5 % skimmed milk, for 1 h at room temperature. Primary antibody incubation was performed overnight at 4 °C. The following day, membranes were washed with 1× TBST and incubated with anti-mouse-IRDye-680RD (#926–68,072) or anti-rabbit-IRDye-800CW (#926–32,211) both from Licorbio diluted (1:5000) in 5 % milk TBST for 1 h at room temperature. Blots were imaged using Odyssey imager (Licorbio). Densitometry analysis was performed with ImageJ (NIH). Primary antibody dilutions were as follows: phospho-GSK3 (1:1000, (#9331S, Cell Signalling), GSK3-total (1:2000, #44–610, ThermoFisher), phospho-AKT-Ser473 (1:1000, #9271, Cell Signalling) and total AKT (1:1000, #9272, Cell Signalling).

2.8. Brain homogenization and protein extraction

Hippocampi and NAc underwent heat stabilization using Stabilizor™ T1 (Denator AB, Sweden). An amount 10 times more than the weight of the sample of Lysis buffer (8 M Urea/ 100 mM AMBIC) was added to each sample supplemented with phosphatase and protease inhibitors (Sigma-Aldrich, St. Louis, USA). Tissue was sonicated for 20 s on ice in small PCT MicroTubes for Barocycler NEP2320 (Pressure BioSciences, USA). Homogenized samples were processed according to Pressure Cycling Technology using Barocycler NEP 2320 (Pressure BioSciences, USA), using a program of 50 s high pressure (35,000 p.s.i.) and 10 s ambient pressure (14.7 p.s.i.) for 60 cycles to guarantee the total disruption of the membranes and efficient protein extraction (Olszowy et al., 2013). The solution was then transferred into a 1.5 ml tube and centrifuged at 16000 x*g* for 1 h at 4 °C. Supernatant, containing only proteins, was transferred to a clean tube and protein quantification was performed using Total Protein Kit, Micro-Lowry, Peterson's Modification (Sigma-Aldrich, St. Louis, USA).

2.9. SDS-page and protein digestion

All the chemicals for Mass Spectrometry analysis are from Sigma-Aldrich (St. Louis, USA). A total amount of 200 µg of protein extract from Hippocampi and NAc were loaded onto 12 % TGX Criterion Gel (Bio-Rad Laboratories, Hercules, Ca, USA) for in-gel proteomic analysis. Proteins were electrophoresed in the gel for 20 min. Gels were washed in milliQ water, stained for 30 min with GelCode (Bio-Rad Laboratories, Hercules, Ca, USA) and de-stained overnight in milliQ water. Each lane was then manually sliced. Gel slices were de-stained 3 times in 25 mM AMBIC/50 % ACN and dried in a vacuum centrifuge (Speedvac, Thermo Scientific, Germany). Samples were reduced (10 mM DTT/100 mM AMBIC, 1 h at 56 °C), alkylated (55 mM IAA/100 mM AMBIC, 45 min at room temperature in the dark) and washed twice with 100 mM AMBIC and dehydrated using ACN. Samples were dried in the Speedvac. Slices were rehydrated with 12.5 µg/ml modified porcine trypsin (Promega, Madison, WI, USA) freshly diluted in 50 mM AMBIC and the digestion was performed overnight at 37 °C. Peptides were eluted twice using 75 % ACN/ 5 % FA, dried in the Speedvac (Thermo Fisher Scientific) until complete dryness and dissolved in 0.1 % FA before further analysis.

2.10. Phospho-peptide enrichment

Peptides were phospho-enriched using TiO_2 beads (TiO_2 Mag Sepharose, GE Healthcare, Little Chalfont, Buckinghamshire,UK) according to manufacturer's instructions and dried in the Speedvac (Thermo Fisher Scientific) until completely dry.

2.11. LC-MS/MS and data acquisition

Dry peptides were re-suspended in 0.1 % FA and separated using a 2D Eksigent nano-LC system (Eksigent, Dublin, CA, USA) coupled to an LTQ-Orbitrap XL mass spectrometer (Thermo Fisher Scientific) operated in DDA mode. Unassigned charge states and singly charged ions were excluded from fragmentation. The dynamic exclusion list was limited to a maximum of 500 masses with a maximum retention time of 2 min and a relative mass window of 10 ppm. Xcalibur software version 2.0.7 (Thermo Fisher Scientific, Germany) was controlling the HPLC, mass spectrometer and data acquisition.

2.12. Mass spectrometry data analysis and data pre-processing

LC-MS/MS raw files were analysed in MaxQuant (Cox 2008, PMID: 19029910) 1.6.17.0 against *Mus musculus* FASTA file with isoforms downloaded from UniProt (Uniprot in 2023 pmid 36408920). Cysteine carbamidomethylation was set to fixed modification, and methionine oxidation, n-terminal protein acetylation and serine, threonine, tyrosine phosphorylation were set as variable modifications. MaxQuant's Match between run function was turned on. The resulting phospho (STY) table was processed in Perseus 1.6.15.0 (The Perseus computational platform for comprehensive analysis of (proteomics data pmid 27348712). Rows that did not have 50 % non-missing values in at least one condition were filtered away. Reverse and potential contaminant sites were filtered away. Raw site intensity values were log2 transformed and column median was subtracted from each sample, and median of all values before subtraction was added to all values to bring the values back to original scale. Missing values were imputed with Perseus replace values from the normal distribution function in total matrix mode. The values were back transformed for subsequent bioinformatics analyses. Data are available via ProteomeXchange (PRIDE database) with identifier PXD060057.

2.13. Bioinformatics analysis

The MS/MS data was analysed using the PhosPiR analysis pipeline (Hong et al., 2022). PhosPiR is an automated proteomics/phosphoproteomics pipeline that performs differential expression analysis, pathway enrichment analysis and network analysis. All output is provided with comprehensive statistics. We compared the phosphosite intensities from hippocampus and nucleus accumbens of mice treated with TAT or DJNKI-1 using PhosPiR's statistic's package utilizing ROTS statistical test (Elo et al., 2009; Hong et al., 2022). For heatmaps, euclidean distance and ward.D2 cluster analysis was applied using the pHeatmap package in R. For visualization, a circosplot of significantly changing phosphosites annotated according to functional groups was created using the "circlize" package in R (Gu et al., 2014).

2.14. Pearson's correlation analysis

Correlation plots were made for mass spectrometry (MS) and behavioural data. Data was separated into four groups, hippocampus treated with TAT ($n = 6$), hippocampus treated with DJNKI-1 (n = 6), nucleus accumbens treated with TAT ($n = 4$), and nucleus accumbens treated with DJNKI-1 ($n = 3$). MS data consisted of phosphosite intensity values, and behavioural data consisted of time scores in seconds for the EPM and light/dark behaviour tests. Pearson correlation was performed to explore the correlative relationship between behaviour and phosphorylation changes for treatment groups. Correlations between proteins for each treatment group was also compared. Pearsons's correlation coefficients and corresponding *p*-values were calculated using R packages ("*stats*" and "*ggcorrplot*", respectively). Correlation of behaviour data verses MS data was plotted using the *ggcorrplot* package, where a threshold of inclusion was set at correlation value of >0.5 in absolute value, and p-value of <0.05 for correlation. Phosphosites that had at least 1 correlation fitting these criteria with any of the 5 behaviour scores were plotted. For these phosphosites, all behaviour correlations were included, even if the correlation coefficient was lower than 0.5. Correlation of protein verses protein was plotted using the "*corrplot*" package. The same statistical significance threshold was applied using

ROTS statistical test *p*-value 0.05 cut off. Only significant correlations are represented (by colored circle) in the plot. The phosphoprotein cross-correlations were ordered using spectral clustering performed using the "spectrum" package in R. Normalized graph Laplacian was calculated from the correlation similarity matrix to generate the eigensystem, then k-means was applied on the top k eigenvectors to get the spectral clusters.

2.15. Responder/non-responder split

From the DJNKI-1 treatment group, we further separated the data into responder and non-responder groups based on the light dark test results. Mice with time spent in the light measuring greater than 1 standard deviation above the mean of TAT-treated mice, were considered responders, while the rest JNKI-1 treated mice were considered non-responders. This left 6 control TAT treated mice and 3 mice in each of the categories responder and non-responder. Separate correlation to light/dark behaviour features and correlation *p*-values are calculated for responders and non-responders. A volcano plot was created with the "ggplot2" package in R to visualize the correlation values and correlation p-value of each phosphoprotein from both responders and non-responders. It should be noted that when the responder/non-responder split analysis was performed on the EPM test results, the split was 2 responders to 4 non-responders, therefore the correlations shown are only valid for correlation with a low anxiety phenotype in the light dark test.

2.16. Motif analysis

Potential GSK3 phoshorylation sites were identified with Perseus motif linear motif analysis tool. Consensus motif $S/TX_{(2-3)}S/T,X/P$ was used to find potential GSK3 sites that were significantly changing (FC > 1.5 and ROTS p-value <0.05). Potential GSK3 sites were required to have a second significant (FC > 1.5 and ROTS p-value <0.05) co-

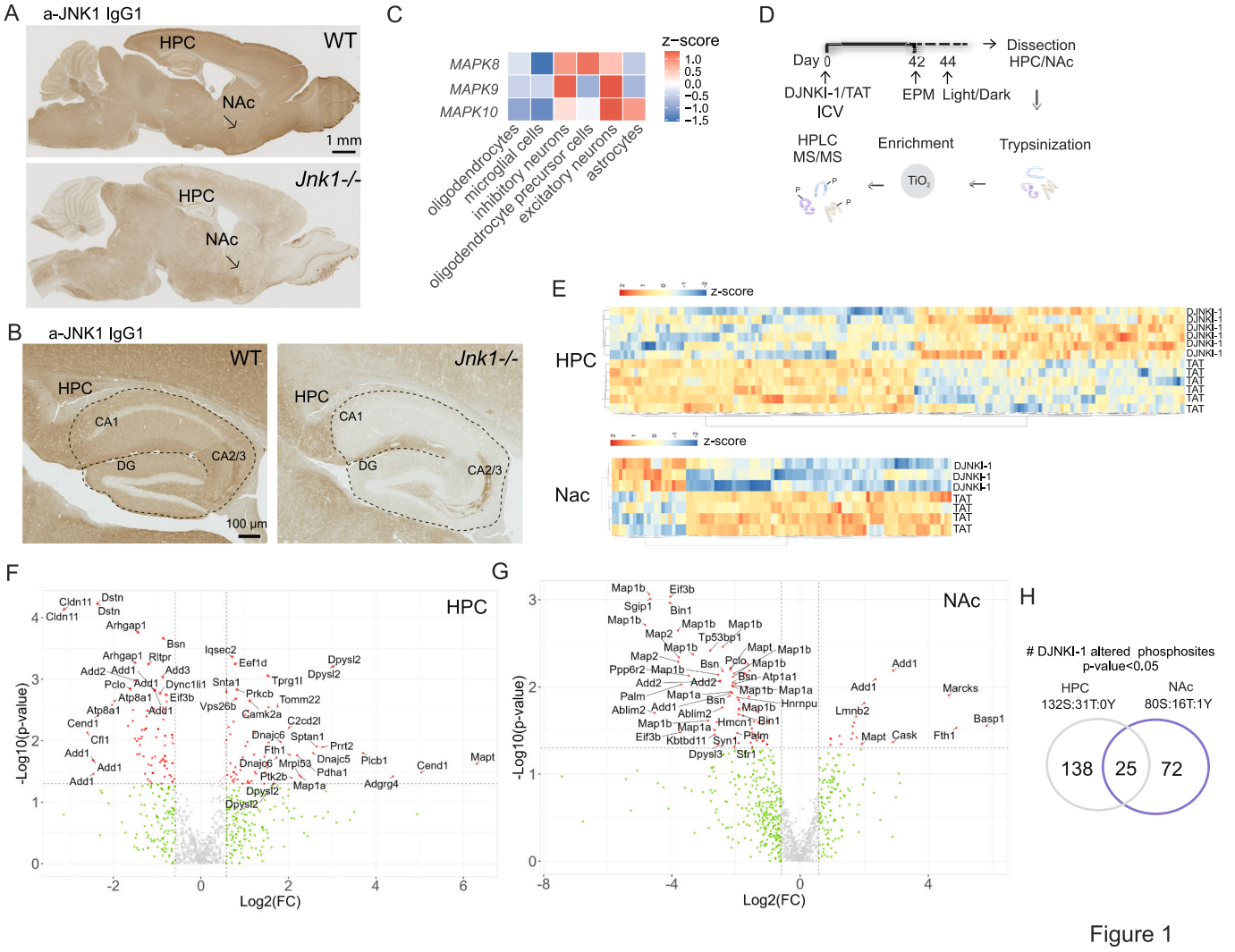

Figure 1

Fig. 1. ICV infusion with DJNKI-1 induces phosphorylation changes in hippocampus and nucleus accumbens. A, B) Sagittal sections from wild type (WT) and *Jnk1−/−* mouse brains stained with antibody against JNK1. Immunohistochemistry reveals the expression of JNK1 in WT brain. Signal specificity is validated using *Jnk1−/−* brain. C) Single cell mRNA levels per cell type cluster were extracted from the Human Protein Atlas database. D) Experimental timeline: mice were infused with DJNKI-1 or TAT for 6 wk. followed by EPM and light/dark behaviour testing. Hippocampus (HPC) and nucleus accumbens (NAc) were dissected and underwent phosphoproteomic investigation. E) Euclidean distance and ward.D2 cluster analysis heatmaps show z-score phosphosite intensities for significant changes (ROTS *p*-value $p < 0.05$) in HPC and NAc. F, G) Volcano plots of phosphosite intensity changes in HPC and NAc following DJNKI-1 treatment. Phosphosites with ROTS p-value<0.05 are red, "*" means ROTS FDR < 0.05. H) The number of significantly changing phosphosites with p-value<0.05 are shown for HPC and NAc. HPC: TAT: $n = 6$, DJNKI-1: n = 6; NAc: TAT: $n = 4$, DJNKI-1: $n = 3$. (For interpretation of the references to colour in this figure legend, the reader is referred to the web version of this article.)

detected on same peptides.

2.17. Single cell data analysis

Tissue data was downloaded from the Human Protein Atlas (Karlsson et al., 2021), and quantitative data for *MAPK8, MAPK9, MAPK10* was extracted. Normalized transcripts (per million) for single cell clusters mapping to excitatory neurons, inhibitory neurons, astrocytes, microglial cells, oligodendrocyte precursor cells and oligodendrocytes were averaged on a per cell basis. *Z*-scores for each gene level per cell type was obtained and plotted.

3. Results

3.1. Intracerebral infusion with JNK inhibitor induces phosphorylation changes in mouse hippocampus and nucleus accumbens

We had previously demonstrated that intracerebral infusion with the DJNKI-1 peptide inhibitor of JNK (Borsello and Bonny, 2004) induces anxiolytic-like behaviour in mice after six weeks, as does genetic deletion of *Jnk1* (Mohammad et al., 2018). Here, we set out to determine the phosphoproteome changes elicited by this inhibitor treatment in the mouse brain. We first examined the localization of constitutively active JNK1 in brain using an antibody with demonstrated specificity by immunoblotting (Coffey et al., 2000; Coffey et al., 2002). JNK1 signal was detected throughout the cortex and subcortical regions, with the most prominent signal in the hippocampus formation, particularly in the neuropil. The staining specificity was confirmed by carrying out labelling in *Jnk1* knockout brain (Fig. 1A, B). Cell type expression of all three *JNK* genes from human brain transcriptomics is shown. JNK1 is enriched in oligodendrocytes and JNKs 2 and 3 in excitatory neurons (Fig. 1C) (Karlsson et al., 2021). Given the high level of JNK1 in the hippocampus (HPC), a region integral to emotional regulation, we focused our analysis there. The nucleus accumbens (NAc), a key region for reward and motivation, was included for comparison.

We next infused mice for six weeks with either DJNKI-1 or the TAT delivery peptide (control), as previously described to elicit an anxiolytic response (Mohammad et al., 2018). Mice subsequently underwent EPM and light/dark tests to assess anxiety-like behaviours. The HPC and NAc were then isolated for phosphopeptide enrichment and LC-MS/MS analysis (Fig. 1D). We identified 992 phosphosites in total. Of these, 163 were regulated by DJNKI-1 in the HPC ($p < 0.05$) (Fig. 1E-G; Supplementary Table 1). Only 25 of the regulated phosphosites overlapped between regions (Fig. 1H, Table 1). These included presynaptic regulators of neurotransmitter release (basoon and piccolo), proteins controlling lipid dynamics (phospholipid-transporting ATPase 1A, paralemmin-1), and cytoskeletal proteins (MAP2, MAP1a, DPYSL3, ADD1 and 3).

Most of the identified sites were not yet functionally annotated, though there were some exceptions. Namely, DJNKI-1 decreased phosphorylation of NDRG2-S332 in the hippocampus (Table 1). NDRG2 (N-myc downstream regulated protein-2) expression is induced by ischemic stress and functions in autophagy regulation (Azad et al., 2025), similar to JNK (Coffey, 2014; Rui et al., 2007). Serine-332 is a priming site for phosphorylation by GSK3 (Murray et al., 2004). Similarly, DPYSL3 (CRMP4) phosphorylation at S522 was decreased in the HPC of DJNKI-1-treated mice (Table 1). This site is phosphorylated by GSK-3, and supports axon growth (Cole et al., 2006) (Table 1).

To gain an overview of the functions of DJNKI-1-regulated phosphoproteins, we plotted the top 20 most significantly changing phosphosites from HPC and NAc in a Circos plot, using functional categories (Fig. 2). Cytoskeletal proteins, especially microtubule stabilizers MAP1a, MAP1b and MAP2 showed large, negative fold-change. MAP1b-S1260, critical for axon collateral branching (Scales et al., 2009; Ziak et al., 2024), was significantly altered in both NAc and HPC. Thirteen additional MAP1b sites were regulated exclusively in NAc (Fig. 2A, Supplementary Table 1). MAP2 phosphorylation decreased at S1352 and T1358 in both regions, with greater reduction in NAc (−13-fold, $p = 0.004$ and 0.005) than HPC (−2.4-fold, $p = 0.006$). Tau (MAPT) S692 (human S717) phosphorylation decreased 4-fold in NAc and 2-fold in HPC. Tau-S692(S717), a site that can be O-glycosylated, influences fibril formation; a hallmark of Alzheimer's (Liu et al., 2004; Pratt and

Table 1
Overlapping phosphorylation sites that changed significantly both in hippocampus (HPC) and nucleus accumbens (NAc).

Protein name (genename: UniProt i.d.)	Residue	HPC FC	p-value	Nac FC	p-value
Bassoon (Bsn; O88737)	S3519	−1.82	0.0002	−4.26	0.00892
Gamma-adducin (Add3; Q9QYB5)	S681	−1.83	0.0009	−2.04	0.04553
Piccolo (Pclo; Q9QYX7)	T3376	−3.06	0.0014	−4.5	0.00606
Dynein 1 light intermediate chain 1 (Dync1li1; Q8R1Q8)	S510	−1.91	0.0017	−2.84	0.02999
Eukaryotic translation initiation factor 3 subunit B (EIF3b; Q8JZQ9)	S75	−1.74	0.0018	−16.55	0.00092
Phospholipid transporting ATPase IA (ATP8a1; P70704)	S29	−3.93	0.0023	−2.44	0.01752
Phospholipid transporting ATPase IA (ATP8a1; P70704)	S25	−4.09	0.0026	−2.23	0.02675
Myc box-dependent-interacting protein 1 (Bin1; O08539)	S296	−1.82	0.0029	−3.79	0.02066
Microtubule-associated protein 2 (MAP2; P20357)	S1352	−2.39	0.0063	−13.74	0.00458
Microtubule-associated protein 2 (MAP2; P20357)	T1358	−2.39	0.0063	−13.97	0.00517
Microtubule-associated protein 1B (Map1b; P14873)	S1260	−2.03	0.0087	−5.31	0.00347
Microtubule-associated protein tau (Mapt; P10637)	S692	−2.45	0.0067	−4.52	0.0063
HSP 90-beta (Hsp90ab1; P11499)	S255	−1.77	0.0119	−1.99	0.0247
Paralemmin-1 (Palm; Q9Z0P4)	S124	−2.74	0.0166	−3.89	0.03375
Ferritin heavy chain (Fth1; P09528)	S5	4.08	0.017	29.32	0.02957
NDRG2 (Q9QYGO)	S332	−1.77	0.0177	−2.96	0.03602
NDRG2 (Q9QYGO)	S338	−1.77	0.0177	−2.71	0.02483
Dihydropyrimidinase-related protein 3 (Dypsl3; Q62188))	S522	−2.48	0.0179	−5.85	0.04636
Dihydropyrimidinase-related protein 3 (Dypsl3: Q62188)	T509	−1.87	0.0209	−3.25	0.00716
26S proteasome non-ATPase regulatory subunit 1 (Psmd1; Q3TXS7)	S315	−1.57	0.0232	−3.03	0.01292
26S proteasome non-ATPase regulatory subunit 1 (Psmd1; Q3TXS7)	T311	−1.57	0.0232	−3.18	0.01844
Catenin alpha-2 (Ctnna2; Q61301)	S654	−2.13	0.0337	−2.99	0.00653
Alpha-adducin (Add1; Q9QYCO-2)	S353	1.76	0.0354	5.11	0.00816
Catenin alpha-2 (Ctnna2; Q61301)	T657	−1.78	0.0385	−2.81	0.04906
Eukaryotic translation initiation factor 3 subunit B (Eif3b; Q8JZQ9)	S79	−2.24	0.0456	−13.31	0.03314

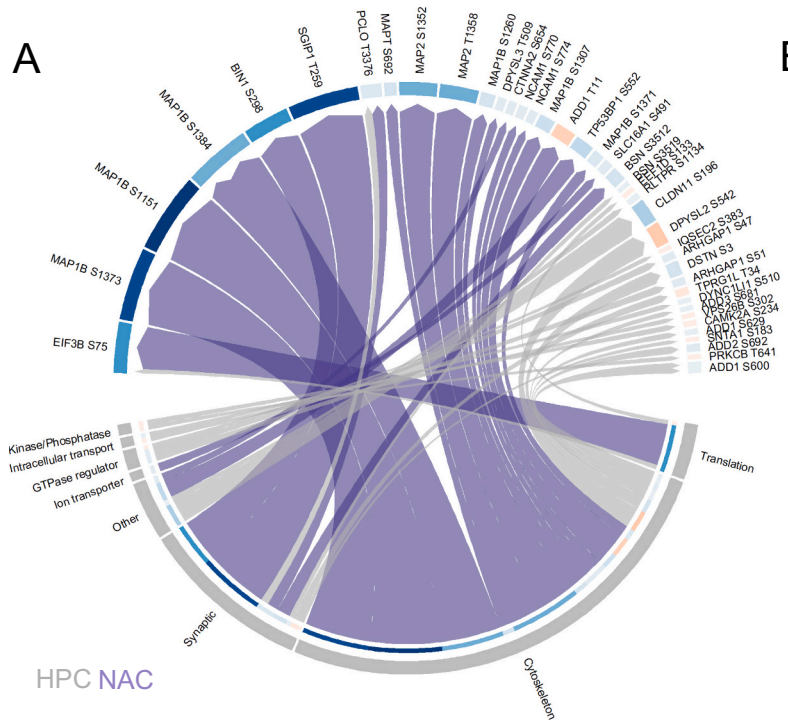

ID	Description	BgRatio	p.adjust	geneID
GO:0051261	protein depolymerization	16/370	0.002	Map1a/Dnajc6/Add3/Stmn1/Evl/Sptbn1/Map2/Map1b/Add1/Add2/Dstn/Cfl1
GO:0043244	regulation of protein-containing complex disassembly	12/370	0.002	Map1a/Add3/Evl/Sptbn1/Map2/Map1b/Add1/Add2/Dstn/Cfl1
GO:1901879	regulation of protein depolymerization	12/370	0.002	Map1a/Add3/Evl/Sptbn1/Map2/Map1b/Add1/Add2/Dstn/Cfl1
GO:0032535	regulation of cellular component size	34/370	0.004	Mapt/Ptk2b/Add3/Evl/Sptbn1/Nefm/Arhgap32/Pclo/Hsp90aa1/Map2/Hsp90ab1/Prkce/Bin1/Map1b/Add1/Add2/Dstn/Cfl
GO:0043242	negative regulation of protein-containing complex disassembly	11/370	0.004	Map1a/Add3/Evl/Sptbn1/Map2/Map1b/Add1/Add2/Cfl1
GO:1901880	negative regulation of protein depolymerization	11/370	0.004	Map1a/Add3/Evl/Sptbn1/Map2/Map1b/Add1/Add2/Cfl1
GO:0032271	regulation of protein polymerization	27/370	0.007	Mapt/Ptk2b/Add3/Tppp/Stmn1/Evl/Sptbn1/Hsp90aa1/Map2/Prkce/Bin1/Map1b/
GO:0032984	protein-containing complex disassembly	19/370	0.007	Map1a/Dnajc6/Add3/Stmn1/Evl/Sptbn1/Map2/Map1b/Add1/Add2/Dstn/Cfl1
GO:0090066	regulation of anatomical structure size	36/370	0.007	Mapt/Ptk2b/Add3/Evl/Sptbn1/Nefm/Arhgap32/Pclo/Hsp90aa1/Map2/Hsp90ab1/Prkce/Bin1/Map1b/Add1/Add2/Dstn/Cfl

Fig. 2. Inhibition of JNK leads to prominent decreases in cytoskeletal protein phosphorylation in both hippocampus and nucleus accumbens. A) Circos plot depicts significantly altered phosphosites with F.C. >1.5, p-value<0.05, grouped by brain region (HPC = grey, NAc = purple) and by functional annotation. Link size and phosphoprotein sector colour correspond to phosphosite intensity F.C. (blue represents decreasing phosphosite intensity and red increasing). Results shown are from the top 20 most significant changes in each brain region. For conciseness, gene names are used. Note DSTN (dystrophin) is otherwise known as cofilin-1 and Bin1 (bridging integrator 1) is otherwise known as amphiphysin-2. B) Gene ontology enrichment of significantly changing phosphoproteins in HPC of DJNKI-1-treated mice. (For interpretation of the references to colour in this figure legend, the reader is referred to the web version of this article.)

Vocadlo, 2023).

Notable in HPC, was a prominent regulation of kinase and phosphatase phosphorylation (Fig. 2; Supplementary Table 1). Significant changes were observed in PRKCB, AAK1, CamK2a, PRKCE, PDPK1, PRTK2b and PP1r7. Among these, PDPK1-S241 phosphorylation, a critical activation loop site that controls its enzymatic activity (Levina et al., 2022), increased 3-fold ($p = 0.0003$), indicating enhanced PDPK1 activity. In contrast, no kinases or phosphatases were significantly altered in NAc. However, several synaptic proteins were regulated in both regions. These included bassoon (Bsn)-S3519 and piccolo (Pclo)-T3376. Synapsin 1 (Syn1), where S427 regulated in HPC, and S568 in NAc (Fig. 2A, Supplementary Table 1).

Gene ontology enrichment analysis highlighted changes to "protein depolymerization and regulation of protein-containing complex disassembly" in the hippocampal DJNKI-1-regulated phosphoproteome (Fig. 2B), with no significant enrichments in the NAc. The Circos plot (Fig. 2A), shows the top 20 regulated phosphoproteins, while additional changes were detected in cytoskeletal regulatory proteins in HPC contributing to this enrichment (Supplementary Table 1).

3.2. *Protein phosphorylation changes in HPC and NAc correlate with high and low anxiety-like behaviours*

We next examined the behaviour of DJNKI-1-treated mice in the EPM and light/dark tests, to replicate the anxiolytic effects previously observed with DJNKI-1 and in *Jnk1−/−* mice (Mohammad et al., 2018). As before, DJNKI-1-infused mice spent more time in the open arms of the EPM and the light area in the light/dark test (Fig. 3A, B). Thus DJNKI-1 treatment induced a similar low anxiety-like phenotype as reported earlier.

To identify which phosphosites were likely to affect the behaviours, we correlated phosphosite intensities with time spent in the aversive and non-aversive zones in the behaviour tests. In control mice, several phosphosites in HPC, including those on tubulin regulatory proteins DPYSL1, 2 and 3 (CRMP1, 2 and 4), as well as adducin 1, correlated bidirectionally with behaviour (Fig. 3C, TAT). Conversely, no such bidirectional correlations were found in the EPM of control mice.

In DJNKI-1-treated mice, an entirely new set of correlations emerged. Altogether 30 phosphorylation sites correlated with time spent in the open/closed arms, and entries to the open arms (Fig. 3C, HPC-DJNKI-1). The correlating phosphosites included axonal proteins regulating actin and microtubules (e.g. MAPT-S695, MAP2-T1358, ANK2-S2364 and SPTBN1-S2164), and synaptic proteins (e.g. BSN-S3519, DSTN(Coflin)-S3 and SNAP91-S296). Notably, destrin (DSTN or cofilin-1)-S3 phosphorylation correlated negatively with time spent in the closed arms of the EPM (Fig. 3C, DJNKI-1). Phosphorylation on this site decreased by 5-fold ($p = 0.00005$) in DJNKI-1-treated mice and was the most significant change in the dataset. Cofilin-S3 phosphorylation has been shown to promote actin filament growth (Mizuno, 2013). Remarkably, in the light/dark test, most correlations disappeared, and only the MAPT-T695 correlation remained. It correlated positively and negatively with time in the dark and light, respectively (Fig. 3C, HPC-DJNKI-1).

In NAc of control peptide-treated mice, fewer significant correlations were observed overall. Notably, MAP2-T1358 phosphorylation correlated with time spent in the open arms in both brain regions after DJNKI-1 treatment, but the correlation was positive in NAc and negative in HPC. We applied spectral clustering to visualize phosphorylation synchronization with or without JNK inhibitor (Fig. 3E). In hippocampus, drug treatment increased the number of clusters of positively correlated phosphoproteins (Fig. 3E), possibly reflecting greater signalling synchronization in HPC when JNK is inhibited.

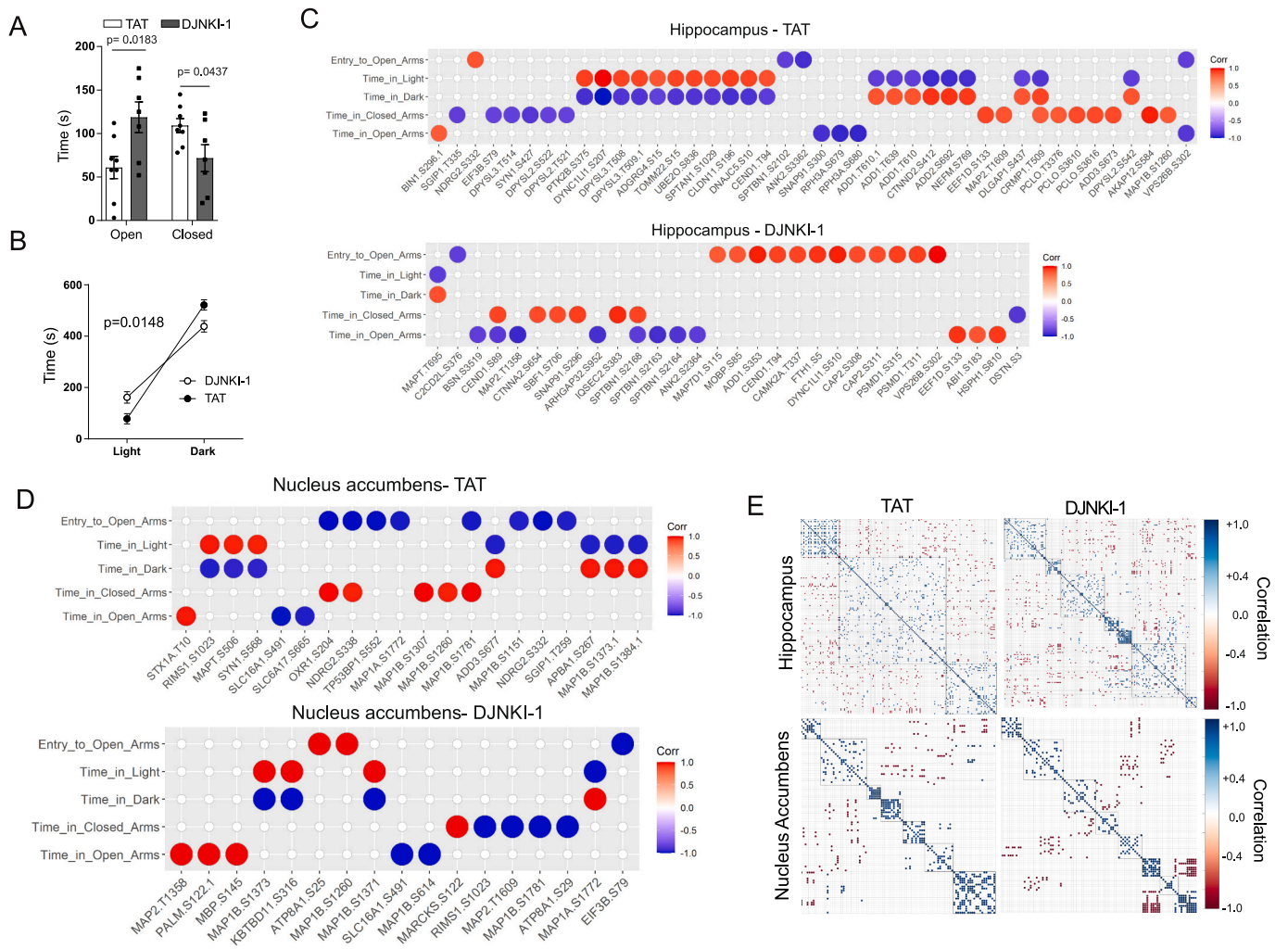

Fig. 3. DJNKI-1 treated mice show reduced anxiety like behaviours that correlate significantly with multiple phosphorylation events in hippocampus. A-B) Behaviour results from the EPM and light-dark test following 6 weeks treatment with TAT (control peptide) ($n = 8$) or DJNKI-1 ($n = 7$). *P*-values were calculated using Student's *t*-test. C) Dot plots show the correlation between behaviours and phosphosite intensities, p-value <0.05 in HPC and NAc. Pearson's coefficients are depicted with red or blue circles for positive and negative correlation respectively. Only correlations >0.5 and p-value <0.05 are included in the plots. E) Spectral clustering of cross-correlated phosphoproteins in HPC and NAc. Only significant correlations ($p < 0.05$) are included. Increased structure or nodes in the cluster pattern are observed upon DJNKI-1 treatment in both regions. (For interpretation of the references to colour in this figure legend, the reader is referred to the web version of this article.)

3.3. *Hippocampus responder/non-responder analysis*

Given that only 50 % of DJNKI-1-treated mice showed an anxiolytic response, we reanalyzed the phosphoproteomic data for responder and non-responder mice separately, to identify phosphorylation changes that were specific for responder mice, and more likely to be linked to behavioural outcome (Fig. 4). Volcano plots depicting phosphorylation changes in the hippocampus of mice that responded to the light/dark test with reduced anxiety "responders", and those that did not "non-responders" are shown (Fig. 4A, B; Supplementary Table 2). Interestingly, the only phosphoprotein that was oppositely regulated in responders and non-responders was NCAM1-S774. It decreased by 3.4-fold ($p = 0.009$) in responders and increased by 2.2-fold ($p = 0.0004$) in non-responders, consistent with it contributing to the behavioural responses. This site regulates NCAM1 interaction with CRMP2 which in turn, promotes calcium and sodium channel stabilization (Chew and Khanna, 2018) (Fig. 6).

There were several unique phosphorylation changes in responder and non-responder mice (Fig. 4A, B). Among these, phosphorylation of adducin-1 T610 and T639 decreased substantially (−20 and − 17-fold, respectively) only in responder mice. On the other hand, MAPT T695 (human T720) increased 125-fold only in non-responder mice. Similarly, Hsp90ab1 phosphorylation decreased −2.5-fold only in non-responders on S255, a site required for apoptosome formation (Kurokawa et al., 2008). Finally, there was a 6-fold increase in phosphorylation of pyruvate dehydrogenase (PDHA1) on S293 in non-responder mice only, indicating inhibition of its activity (Seifert et al., 2007) (Fig. 6).

Several synaptic phosphoproteins were significantly regulated in HPC of responder and non-responder mice (Fig. 4A). Many of these correlated negatively or positively with anxiety-like behaviour following DJNKI-1 (Fig. 4C). In responder mice, piccolo-S1332, amphiphysin-2 (Bin1)-S298, adducin 1-T639, PSD3-S339 and RIMS1-S1027 and S1023 correlated with behaviours (Fig. 4C). Phosphorylation of STX1b-S14 decreased only in responder mice. This site regulates neurotransmitter release (Shekar et al., 2023). In non-responders, phosphorylation of nerve terminal and cytoskeletal proteins (e.g. synapsin I/III, NEFH, MAP2, MAPT, CFL1, DPYSL2) correlated with light/dark test behaviour (Fig. 4C). These findings suggest presynaptic regulators of neurotransmitter release are likely drivers of anxiety-like behaviours.

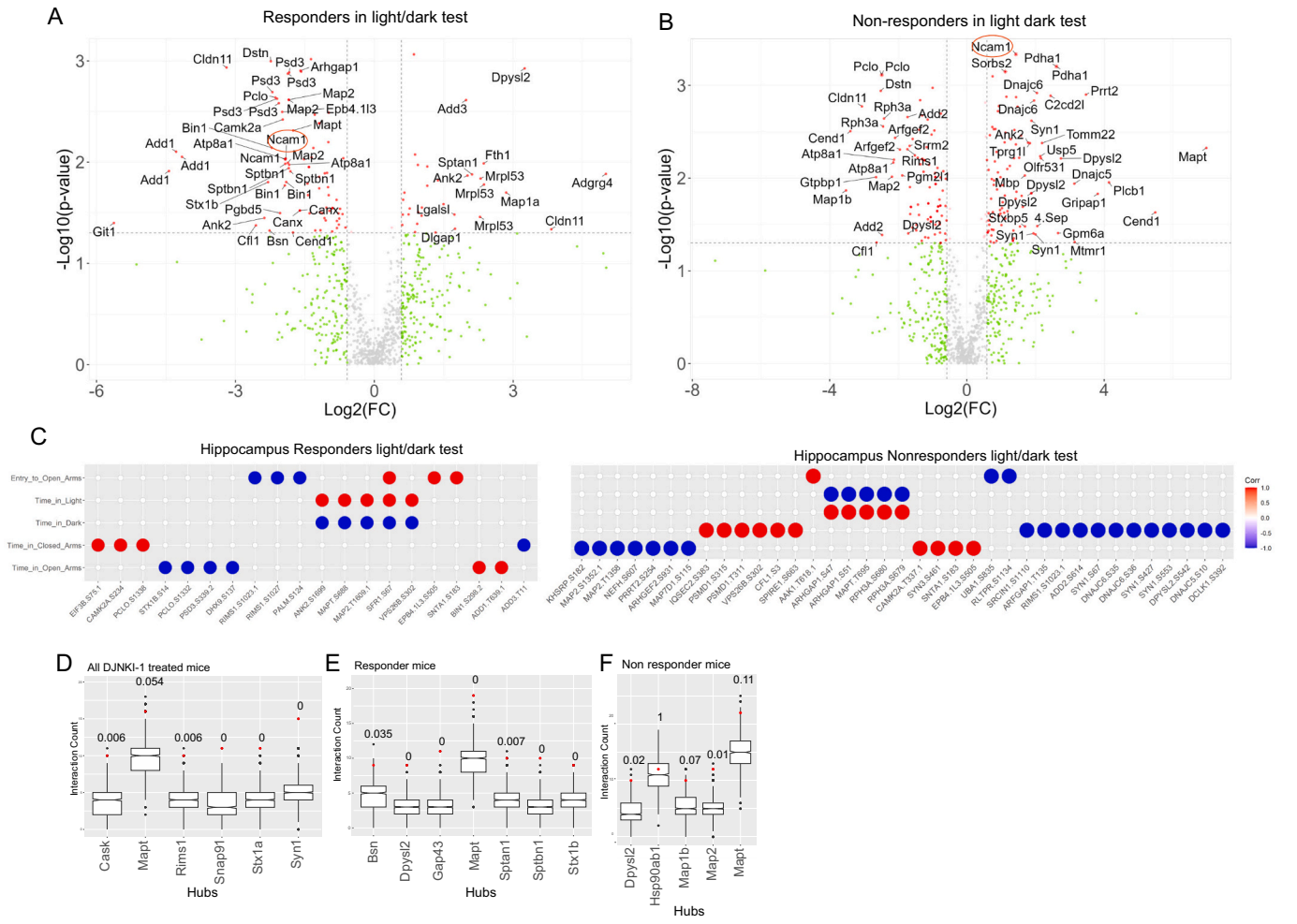

Fig. 4. DJNKI-1-induced phosphorylation changes in responder and non-responder mice. A, B) Volcano plots depict phosphosite changes in responder and non-responder mice compared to control. Phosphosites with ROTS p-value<0.05 are red, "*" means ROTS FDR < 0.05. $N = 6$ for TAT-treated mice and n = 3 respectively for responder and non-responders. C) Correlations plots of significantly changing ($p < 0.05$ using ROTS) phosphosite intensities against behavioural metrics (number of entries to open arms, time in closed or open arms) for the EPM test and (time in the light/dark zones) for the light/dark test are shown. Pearson's correlations for phosphosites p-value <0.05 using the ROTS test are indicated. C) Protein phosphorylation changes that significantly correlate with either low or high anxiety behaviours in light-dark or EPM test are shown. Pearson's r is plotted against $-\text{Log}_2$ p-value. The phosphopeptide list showing corresponding phosphosite information can be found in Supplementary Table 2. D-F) Signalling hub analysis shows the most highly interacting signalling nodes in the phosphoproteomes of DJNKI-s-treated mice (D), responder mice (E) and non-responder mice (F). Horizontal black lines depict the median values for number of interacting proteins based on bootstrapping against all phosphoproteins identified in HPC. The red spot indicates the number of putative interacting proteins in the comparison group and the corresponding p-value. (For interpretation of the references to colour in this figure legend, the reader is referred to the web version of this article.)

Signalling hub connectivity increases in the hippocampus of DJNKI-1-treated mice.

To explore the connectivity of DJNKI-1-regulated phosphoproteins, we created interaction networks using the STRING database. Hubs were defined as phosphoproteins with connectivity greater than two standard deviations above the mean interaction count. To validate hub specificity, we generated 1000 random background networks of equivalent size and compared interaction counts to identify statistically significant hubs. Our analysis suggests that CASK, MAPT, RIMS1, SNAP91, STX1A, and SYN1 function as hubs in the phosphoprotein network of DJNKI-1-treated mice (Fig. 4D-F).

Interestingly, when focusing exclusively on responder mice, a distinct set of hubs with significant connectivity emerged. These included DPYSL2 (CRMP2), GAP43, MAPT, spectrin beta (SPTBN1), spectrin alpha (SPTAN1), and STX1B (syntaxin 1b). This pattern suggests more robust hub activity in responder mice following DJNKI-1. These hubs may potentially drive the signalling underlying the low-anxiety phenotype. In contrast, there was no specific signalling hub in the non-responder group, indicating minimal changes in phosphoprotein connectivity relative to the random background networks.

The AKT-GSK3 pathway is regulated in JNK inhibitor-treated mice.

We previously described the phosphoproteome of *Jnk1*−/− mouse brain (Hong et al., 2024), identifying that JNK1 regulates AKT1 and GSK signalling hubs that contribute to anxiolytic behaviours (Hong et al., 2024). We therefore decided to examine GSK3 phosphorylation in our dataset, as GSK3 is independently implicated in anxiety regulation (Crofton et al., 2017; Mines et al., 2010),

GSK3 sites were predicted from the DJNKI-1-regulated hippocampal phosphoproteome using the motif $S/T_{X(2-3)}S/T$, where the priming site is classically C-terminal to the GSK3 site (Fiol et al., 1987). We required both sites to be significantly regulated by >1.5 fold in the same direction. The results, shown in Table 2 reveal that all predicted GSK3 sites underwent negative fold-changes in DJNKI-1-treated mice, along with their predicted priming sites. In total, 18 GSK3 motifs showed decreased phosphorylation in the hippocampus and 10 in the nucleus accumbens (Table 2). Notably, these changes occurred in responder and non-responder mice; however, only 30 % occurred in both regions

Table 2
Potential GSK3 motifs identified from nucleus accumbens and hippocampus of DJNKI-1-treated mice. A "relaxed" GSK3 consensus motif S/TX$_{(2-3)}$S/T,X/P search was applied. Significantly changing phosphosites (FC > 1.5, $p < 0.05$) are shown only in cases where both priming site and GSK3 site (red and green) are altered relative to control, with the exception of MAP1b (with x = 4) and MAPT, both of which are reportedly unprimed GSK3 target sites (PMID; 15731007; 33804962). Sites co-detected by MaxQuant are shown when significant and are bolded black. Miss-cleavage sites are indicated by |. Sites that change with FC > 3 are indicated with a "*". In hippocampus, FC and *p*-values are shown for sites in all mice "A", responder mice "R" and non-responder mice "N". UniProt ID and corresponding gene names are given. Gene names replace protein names. Thus Bin1, Dpysl3 and SPTBN1 are commonly known as amphiphysin-2, CRMP4 and spectrin β.

Protein (gene ID)	UniProt ID	Phosphopeptide sequence Mouse	Phosphosite Mouse	Phosphosite Human	Fold Change	p-value	PMID
GSK3 motifs identified in Nucleus Accumbens							
*Add2	Q9QYB8	PVK*STPASPVQSPSK *TSE	S602/S606	S600/S604	-5.65/-5.62	0.009/ 0.009	n.a.
Add3	Q9QYB5	PER*TEEVLSPDGSPSKSPSK*KKK	S677/S681	S677/S681	-2.04/-2.04	0.046/0.046	n.a.
Atp8a1	P70704	YEK*TDDVSEKTSLADQEEVR*TIF	S25/S29	S25/S29	-2.23/-2.44	0.027/0.018	n.a.
Ctnna2	Q61301	DVR*SRTSVQTEDDQLIAGQSAR*AIM	S654/T657;S655/658	S654/T657	-2.99/-2.81	0.007/0.049	n.a.
*Eif3b	Q8JZQ9	EVR*AKPAAQSEEETATSPAASPTPQSAER*SPS	S75/S79	G75/S83	-16.55/-13.31	0.001/0.033	n.a.
*Map1b	P14873	PAK*SPSLSPSPPSPIEK*TPL	S1255/S1260	S1260/S1265	-7.32/-5.31	0.024/ 0.003	PMID: 15731007
Mapt	P10637	NAK*AK|TDHGAEIVYK|SPVVSGDTSPR*HLS	S692/T695/S696	S717/T620/S721	-1.81/-4.52/-1.47/-6.9	0.006/0.220/0.153	PMID: 30668577
*Ncam1	P13595	EEG*AAFSKDESKEPIVEVR*TEE	S770/S774	S780/S784	-3.25/-3.1	0.005/0.005	n.a.
Psmd1	Q3TXS7	EEK*TASAVAGKTPDASPEPK*DQT	T311/S315	T311/S315	-3.18/-3.03	0.018/ 0.013	n.a.
Sgip1	Q8VD37	PPK*TVPATPPRTGSPLTVATGNDQAATEAK*IEK	T259/T263	T259/T263	-25.58/-2.83	0.001/0.033	n.a.
GSK3 motifs identified in Hippocampus							
Add1	Q9QYC0	KAK*SR|SPGTPAGEGSGSPPK*WQI	S355/T358	S355/S358	A: -1.97/-1.97 N: -2.18/-2.18	A: 0.006/ 0.006 N: 0.019/0.019	n.a.
Arhgap1	Q5FWK3	FPK*SDDSKSSSPEPVTHLK*WDD	S47/S51	S47/S51	A: -2.71/-2.84 R: -3.02/-2.99 N: -2.47/-2.7	A: 0.000/0.001 R: 0.001/0.001 N: 0.002/0.006	n.a.
*Atp8a1	P70704	YEK*TDDVSEKTSLADQEEVR*TIF	S25/S29	S25/S29	A: -4.09/-3.93 R: -3.8/-3.58 N:-4.42/-4.36	A: 0.003/0.002 R: 0.009/0.011 N: 0.007/0.006	n.a.
*Bin1	O08539	PEK*GNKSPSPPPDGSPAATPEIR*VNH	S296/S298/S304	S298	R: -3.74/-3.82	R: 0.016/0.017	n.a.
Ctnna2	Q61301	DVR*SRTSVQTEDDQLIAGQSAR*AIM	S654/T657	S654/T657	A: -2.13/-1.78 R: -2.18/ -2.26	A: 0.034/0.038 R: 0.032/0.031	n.a.
Dpysl3	Q62188	VPR*GMYDGPVFDLTTTPK|GGTPAGSTR|GSPTRPNPPVR*NLH	T509/T514	T509/T514	A: -1.87/-1.86 N: -2.47/-1.72	A: 0.021/0.050 N: 0.006/0.039	15466863
Epb4.1l1	A2AUK5	RER*RLPSSPASPSPK|GTPEK*ASE	S546/T550	S546/T550	N: -1.82/-1.82	N: 0.023/0.023	n.a.
Eif3b	Q8JZQ9	EVR*AKPAAQSEEETATSPAASPTPQSAER*SPS	S75/S79	G79/S83	A: -1.74/-2.24 N: -2.00/-2.78	A: 0.002/0.046 N: 0.001/0.037	n.a.
Map1b	P14873	PAK*SPSLSPSPPSPIEK*TPL	S1255/S1260	S1260/S1265	N: -11.49/-2.4	N: 0.014/0.009	15731007
Mapt (Tau)	P10637	NAK*AK|TDHGAEIVYK|SPVVSGDTSPR*HLS	S688/S692	S713/S717	R: -1.75/-3.37	R: 0.038/0.005	33804962
*Ncam1	P13595	EEG*AAFSKDESKEPIVEVR*TEE	S770/S774	S780/S784	R: -3.79/-3.77	R: 0.009/0.009	n.a.
Nefh	P19246	DVK*AKPLDVKSPEAQTPVQEEAK*HPT	S834/T839	S764/T768	A: -2.63 /-2.64 R: -2.28/-2.28 N: -3.10/-3.14	A: 0.012/0.016 R: 0.004/0.004 N: 0.020/0.024	n.a.
Pclo	Q9QYX7	LKK*DSFSQESSPSSPSDLAK*LES	S1332/S1338	S1396/S1402	R: -1.61/-1.71	R: 0.033/0.032	n.a.
Ppp1r7	Q3UM45	VDR*RVESEESGDEEGKK*HGG	S24/S27	S24/S27	A: -2.33/ -2.33 R: -2.66/-2.66 N: -2.07/ -2.07	A: 0.003/0.003 R: 0.011/0.011 N: 0.029/0.029	n.a.
Psmd1	Q3TXS7	EEK*TASAVAGKTPDASPEPK* DQT	T311/S315	T311/S315	A: -1.57/-1.57 N: -1.88/-1.88	A: 0.023/0.023 N: 0.012/0.012	n.a.

simultaneously. These findings suggest that GSK3 signalling is inhibited in these brain regions following DJNKI-1 treatment.

GSK3β is inhibited by JNK inhibitor treatment or *Jnk1* deletion *in* HPC and NAc.

We assessed whether DJNKI-1 treatment altered GSK3 activity using phospho-antibodies recognising the activation state of GSK3α and β. Eight hours treatment of cortical neurons with DJNKI-1 (20 μM) inhibited both GSK3 isoforms (Fig. 5A-C). We also measured the activity of AKT, which inhibits GSK3α and β by direct phosphorylation on S21 and S9, respectively. AKT-S473 phosphorylation increased, indicating activation (Fig. 5A, D). Similar regulation of GSK3β and AKT activity was observed in the NAc of *Jnk1−/−* mice (Fig. 5E-H). These results indicate that inhibition of JNK in the mouse brain activates AKT and inhibits GSK3 activities.

3.4. DJNKI-1 treatment regulates insulin/glucose pathway regulation, including pyruvate dehydrogenase inhibition

Fig. 5L summarizes the DJNKI-1-regulated phosphosites identified in this study that control energy metabolism. We identify that in DJNKI-1-treated mouse hippocampus, PDK1-S244 (S241 in human) phosphorylation increases, indicating enzymatic activation (Levina et al., 2022). Consistent with this, the downstream target of PDK1, PRKCB-T641 also increases, indicating elevated activity (Zhang et al., 1994). Another downstream target of PDK1, PDHA1-S293 undergoes increased phosphorylation, signifying enzymatic inhibition (Seifert et al., 2007). The net effect of these events is an expected block of oxidative phosphorylation. Downstream of PDK1 activation, we identify that AKT is activated and GSK3 inhibited. Consistent with this, GSK3 phosphorylation motifs identified in hippocampus show reduced phosphorylation. These GKS3 regulated phosphoproteins are involved in synaptic plasticity, adhesion, cytoskeletal changes and proteostasis (Fig. 5L). Fig. 6 provides a detailed summary of the synaptic proteins that are regulated by DJNKI-1. Information on the regulation of these sites overall and in responder and non-responder mice is found in supplementary tables 1 and 2.

4. Discussion

Deciphering the underlying mechanisms of neurological disorders requires understanding of protein phosphorylation changes in the brain. Here we analyse phosphoproteomic changes in the hippocampus of mice undergoing anxiety-inducing behavioural tests in the presence or absence of an anxiolytic agent; JNK inhibitor DJNKI-1. This highlights potential cellular mechanisms through which JNK activity may contribute to aversive behaviours.

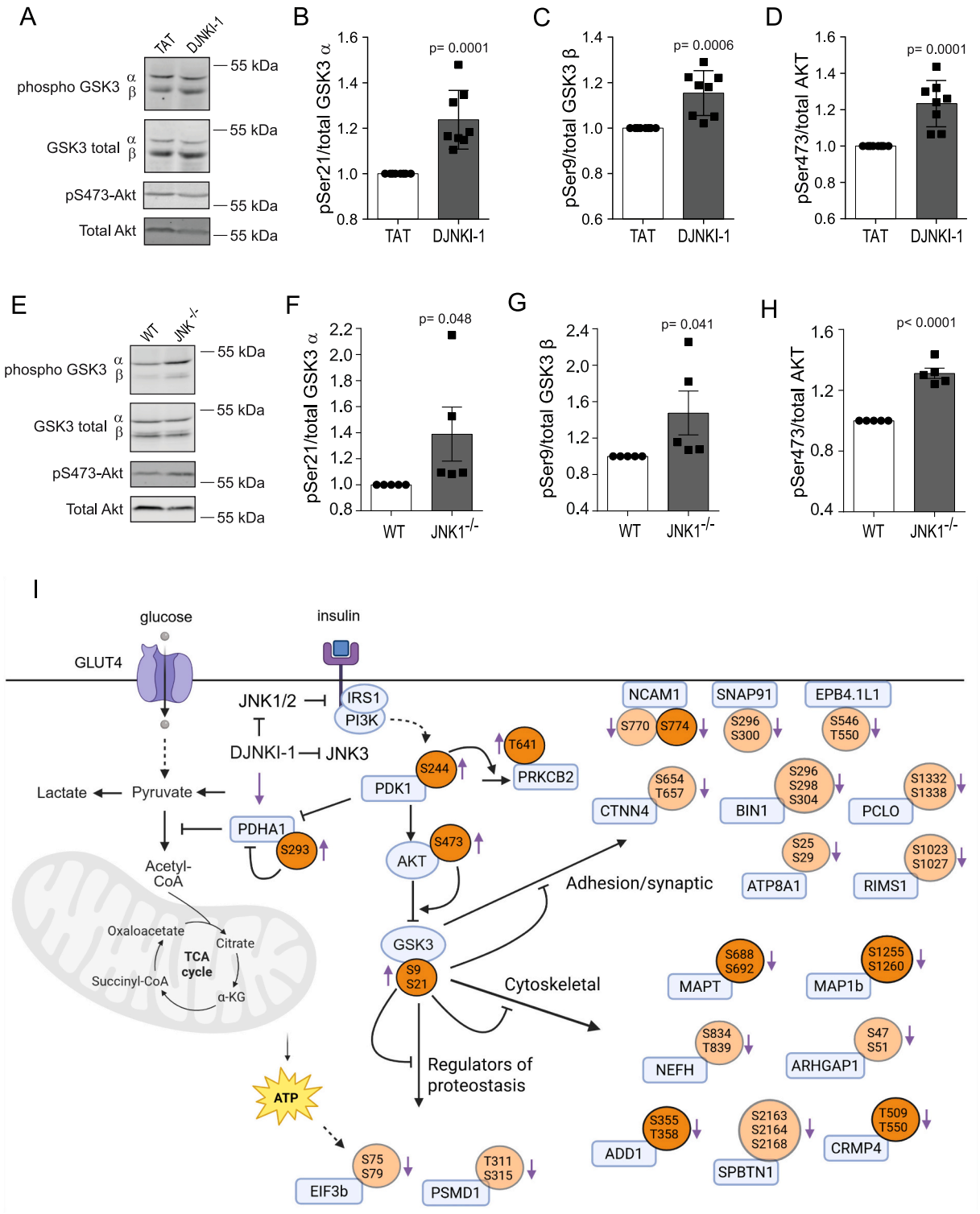

Fig. 5. DJNKI-1 regulates many enzymes controlling energy metabolism. A-C) Cortical neurons at 16 days in vitro were treated with DJNKI-1 (20 μM) or TAT carrier (20 μM) for 8 h. Phosphorylation of GSK3 on Ser9 or Ser21 is shown. Phosphorylation of GSK3α/β increases following DJNKI-1 indicating decreased activity. D) Quantitative data for phospho-Ser473-AKT is shown. *E*-H). Representative blots and quantitative analysis for GSK3α/β and AKT phospho-blotting in NAc of wild-type (WT) and *Jnk1−/−* mice. Error bars represent standard errors of the mean. Significance was analysed by t-test. I) The scheme summarizes the DJNKI-1-regulated phosphoproteins that are involved in insulin signalling, including those that are regulated on GSK3 motifs. Annotated phosphosites are deep orange, unannotated sites are pale orange. The curly line indicates the effect of a given phosphorylated site on protein function, where known. The vertical purple arrows indicate the direction of phosphorylation change following DJNKI-1 treatment. Accompanying meaned data with FC and *p*-values are found in Supplementary tables 1 and 2. Images from all immunoblots used in the study are in Supplementary data 3. (For interpretation of the references to colour in this figure legend, the reader is referred to the web version of this article.)

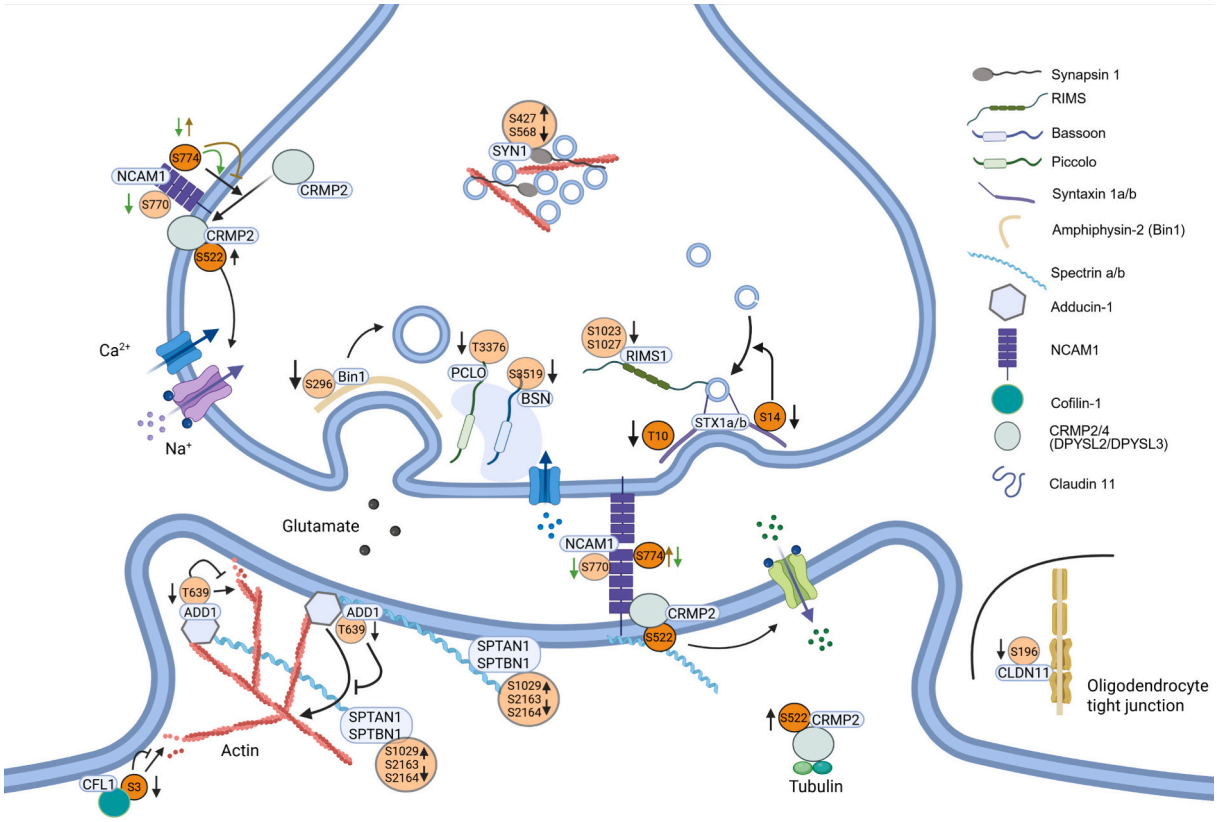

Fig. 6. JNK-regulated phosphorylation of synaptic proteins. A scheme depicting the examples of synaptic proteins that are regulated by DJNKI-1 in this study. Phosphosites with annotated function are highlighted in deep orange. Curly arrows indicate the effect of a given phosphorylated site on protein function, where known. The directionality of DJNKI-1-regulated phosphorylation change, increased or decreased, is indicated by vertical arrows in DJNKI-1-treated mice. For NCAM1, green/brown arrows represent responder/non-responder phosphorylation change. Accompanying data is found in Supplementary tables 1 and 2. (For interpretation of the references to colour in this figure legend, the reader is referred to the web version of this article.)

In this study, we e identify that JNK inhibition imposes large-fold changes on the phosphorylation of microtubule associated proteins (MAPs), especially MAP1A/B and MAP2. These proteins are vital for axon and dendrite stability as well as protein transport (Chakraborti et al., 2016; Dent, 2020), and MAP1B and MAP2 are also expressed in glial cells, where they influence cytokine release (Adrian et al., 2023). In brains from individuals with bipolar depression or schizophrenia, alterations in the abundance or phosphorylation of MAPs has been associated with the pathology (Marchisella, 2016). Here, inhibiting JNK decreases the phosphorylation of multiple sites on MAPs in both hippocampus and nucleus accumbens, by up to −28-fold. One such site is MAP2-S1783 (human S1782), which DJNKI-1 decreases. Phosphorylation on this site is increased in schizophrenic brain, where it is reported to alter dendrite architecture (Grubisha et al., 2022). We also find that phosphorylation of MAP1B-S1260 (human T1265) is similarly reduced in hippocampus and nucleus accumbens (−2-fold, $p = 0.008$; −5-fold, $p = 0.003$, respectively). This site controls axon branching and spacing (Scales et al., 2009; Ziak et al., 2024). Interestingly, axonal branching is reduced in adult brain by chronic stress and has been associated with anxiety and depression (Shimada et al., 2024). Several additional sites on MAP1B are also regulated, namely S11373, S1151, S1384, S1307, S1371, S1373 and S1781, that decrease by as much as −25-fold in nucleus accumbens. These findings extend earlier findings on JNK1-dependnet phosphorylation of MAPs and axodendritic architecture (Björkblom et al., 2005; Chang et al., 2003; Komulainen et al., 2014; Teng et al., 2001). Moreover, our findings indicate that JNK acutely regulates MAP phosphorylation in the adult brain, independent of its developmental function.

Synaptic protein phosphorylation is highly regulated by DJNKI-1 in this study. Adducin-1 is a post-synaptic protein that undergoes robust dephosphorylation on several sites upon JNK inhibition (up to −22-fold). This occurs only in hippocampi of responder mice suggesting a role in JNK-mediated aversive behaviour. Adducin 1 phosphorylation promotes assembly of the spectrin-F-actin network and stabilizes synapses. Accordingly, *Add1*−/− mice exhibit increased filopodial turnover in the hippocampus (Bednarek and Caroni, 2011; Pielage et al., 2011). Similarly, *Jnk1*−/− mice exhibit increased thin spine density in hippocampus, and impaired acquisition learning (Komulainen et al., 2020).

The most significantly changed phosphosite in this study is cofilin-1 (DSTN/dystrophin)-S3, which is reduced by 5-fold. Phosphorylation of this site stabilizes actin filament growth and promotes mature spine formation (Ben Zablah et al., 2020; Mizuno, 2013). Thus, cofilin-S3 phosphorylation and adducin-1 phosphorylation by JNK both mediate actin filament/network growth and represent novel mediators of JNK action on the actin cytoskeleton. They may for example contribute to JNK-mediated internalization of AMPA receptors and spine retraction, in response to glucocorticoid stress (Gu et al., 2010; Hollos et al., 2020; Komulainen et al., 2020; Thomas et al., 2008). Notably, cofilin is also expressed pre-synaptically where it may regulate neurotransmitter release (Ben Zablah et al., 2020).

Another novel downstream target of JNK in this study is claudin-11-S196. Expression of claudin-11 is enriched in myelin-producing, oligodendrocyte cells. Thus, claudin-11 is an integral tight junction protein, that affects myelin structure. It is present at tight junctions of the choroid plexus epithelium, and contributes to blood brain barrier tightness (Uchida et al., 2019). Notably, JNK has been shown to deregulate tight junctions via a mechanism involving adducin-1, and JNK inhibition restores tight junction integrity (Wang et al., 2015).

Claudin-11 is an interesting new downstream target of JNK, which like JNK1 and adducin-1, shares the low anxiety phenotype when the gene is knocked out (Maheras et al., 2018). In *claudin-11* knockouts, myelinated axons exhibit slower transmission time. These data highlight a potential role for oligodendrocyte tight junction regulation downstream of JNK.

We also find that phosphorylation of SNARE proteins, syntaxin-1a and b, is reduced in the hippocampus of DJNKI-1-treated mice. Notably, syntaxin-1b-S14 changes in responder mice only, suggesting that it may contribute to JNK mediated aversive behaviour. Syntaxin-1 mediates the fusion of synaptic vesicles with the plasma membrane, thereby facilitating neurotransmitter release (Jahn et al., 2024). The S10 and S14 sites reside within the MUNC18 binding domain, which is required for fusion (Rickman and Duncan, 2010; Yang et al., 2023). Phospho-mimetic syntaxin-1 S14 is reported to prevent interaction with MUNC18 and impair exocytosis (Rickman and Duncan, 2010; Shi et al., 2021). However, syntaxin-1b-S14 phosphorylation is also reported to increase non-evoked release (Shekar et al., 2023). JNK activity, on the other hand, is reportedly required for both spontaneous and Ca^{2+}-evoked neurotransmitter release (Abrahamsson et al., 2017; Biggi et al., 2017; Mori et al., 2008). Interestingly, in the hippocampus of responder mice, syntaxin-1b-S14 is identified as a central, highly connected hub protein in the phosphoproteome network. Its role as a hub is statistically very robust (FDR = 0), suggesting that it is a key regulator of signalling changes in these mice.

One of the aims of this study was to identify phosphosites that correlate with either responder- or non-responder-type behaviour. Interestingly, we only detect one phosphosite that is oppositely regulated in both groups. This is NCAM1-S774, a site that when phosphorylated facilitates interaction with CRMP2 (DPYSL2) (Karbe et al., 2013). Both proteins share common functions in the regulation of synaptic pruning and synapse stability (Duncan et al., 2021; Ziak et al., 2020). Interestingly, CRMP2-S546 phosphorylation increases 7 and 9 fold respectively, in responder and non-mice, however S522, a functionally characterized site on CRMP2, increases 3.6-fold, only in non-responder mice. Phosphorylation on this site stabilizes sodium channel NaV1.7 and calcium channel CaV2.2 (N-type voltage gated calcium channel) stability at the cell surface, thereby increasing presynaptic excitability (Stratton et al., 2020).

Beyond the known regulation of the insulin pathway by JNK, we detect DJNKI-1-dependent modulation at multiple downstream nodes on this pathway, including key regulators of pyruvate metabolism. This reproduces and extends the already recognised role of JNK in insulin resistance (Aguirre et al., 2002; Hirosumi et al., 2002; Solinas and Becattini, 2017). New in our study, we identify activation of PDPK1 and PRKCB upon JNK inhibition, based on increased phosphorylation of critical sites S244 and T642, respectively. Moreover, DJNKI-1 increases PDHA1 (pyruvate dehydrogenase) phosphorylation on S293 which inhibits its enzymatic function (Seifert et al., 2007). Inhibition of PDHA1 redirects pyruvate towards lactate production rather than oxidative phosphorylation (Seifert et al., 2007). This well characterized metabolic shift in neurons is known as the Warburg effect (Bouzier-Sore et al., 2006; van Hall et al., 2009; Wyss et al., 2011). It may benefit neurons by minimizing production of reactive oxygen species via the TCA cycle. Interestingly, astrocytic lactate reduction is associated with depressive behaviours and lower firing frequency in the medial prefrontal cortex of mice (Yao et al., 2023). Additionally, lactate stimulates hippocampal neurogenesis eliciting an antidepressant effect (Bas-Orth et al., 2017; Benarroch, 2024).

Consistent with these findings on glucose metabolism regulation, we show that GSK3α/β activity is repressed in DJNKI-1 treated mice. Corroborating this, 28 GSK3 motifs are downregulated at the level of phosphorylation, both at the priming site and the GSK3 site. These include well characterized GSK3 target sites; Dpysl3-T514 (Cole et al., 2004), MAP1B-S1260 (Trivedi et al., 2005) and MAPT-S692 (Sayas and Ávila, 2021). Additionally, SPTBN1 (spectrin beta) is linked to GSK3, although the motif has not been validated yet (Shinde et al., 2017). Other DJNKI-1-regulated GSK3 motifs are found on DSTN (dystrophin/cofilin) S3, MAP2 T1620 and T1623, and MAPT S692 (human S717), a site that is implicated in neurofibrillary tangles (Cruz et al., 2003).

Negative regulation of GSK3α/β leads to anti-depressant behaviours as observed in *GSK3β−/−* mice (Ziak et al., 2024). Similarly, silencing of GSK3β in the nucleus accumbens reduces anxiety in rats (Crofton et al., 2017), and GSK3β inhibition by lithium, may contribute to its mood-stabilizing effects (Gould et al., 2004; Li and Jope, 2010; Stambolic et al., 1996), and to the action of antidepressant drugs (Beaulieu, 2012). This regulation of GSK3 by JNK supports te role of GSK3 as a key mediator of the anxiolytic effect of JNK inhibition.

In summary, we demonstrate that JNK regulates the phosphorylation of a wide range of proteins that may contribute to anxiety behaviour. These include synaptic proteins involved in neurotransmission regulation and enzymatic the neuronal Warburg effect. Notably, many of the negatively regulated phosphosites lie within a GSK3 motif, and consistent with this, we show that JNK activates GSK3α/β activity. The data provides an annotated repository of JNK-regulated phosphosites in hippocampus and nucleus accumbens.

CRediT authorship contribution statement

Ye Hong: Writing – review & editing, Visualization, Software, Methodology, Investigation, Formal analysis, Data curation. **Valentina Siino:** Writing – review & editing, Visualization, Formal analysis, Data curation. **Dani Flinkman:** Writing – review & editing, Investigation, Formal analysis. **Prasannakumar Deshpande:** Formal analysis. **Sylvia Ortega Martinez:** Writing – review & editing, Visualization, Methodology, Formal analysis, Data curation. **Veronica Fagerholm:** Writing – review & editing, Visualization, Methodology, Formal analysis. **Artemis Varidaki:** Writing – review & editing, Formal analysis. **Pierre Heemeryck:** Methodology, Formal analysis. **Christel Sourander:** Writing – review & editing, Formal analysis. **Peter James:** Writing – review & editing, Methodology, Conceptualization. **Eleanor Coffey:** Writing – original draft, Supervision, Project administration, Funding acquisition, Formal analysis, Conceptualization.

Ethical statement

Animal procedures were conducted with approval from ELLA, the authority responsible for these procedures in Finland, licence number: ESAVI/1897/04.10.07/2015.

Declaration of competing interest

The authors declare no conflict of interest related to the data presented in this study.

Acknowledgements

This project was funded by grants from the Marie Slodowska Curie Actions r'BIRTH Initial Training Network grant #608346 and the Research Council of Finland grant #310583 to E.C. The schemes in Fig. 5I and 6 were prepared with Biorender software.

Appendix A. Supplementary data

Supplementary data to this article can be found online at https://doi.org/10.1016/j.nbd.2025.107207.

Data availability

Data is on PRIDE

References

Abrahamsson, T., et al., 2017. Differential regulation of evoked and spontaneous release by presynaptic NMDA receptors. Neuron 96, 839–855 e5.

Adrian, M., et al., 2023. Polarized microtubule remodeling transforms the morphology of reactive microglia and drives cytokine release. Nat. Commun. 14, 6322.

Aguirre, V., et al., 2002. Phosphorylation of Ser307 in insulin receptor substrate-1 blocks interactions with the insulin receptor and inhibits insulin action. J. Biol. Chem. 277, 1531–1537.

Antoniou, X., et al., 2011. JNK3 as a therapeutic target for neurodegenerative diseases. J. Alzheimer's Dis 24, 633–642.

Azad, M.G., et al., 2025. NDRG1 and its family members: more than just metastasis suppressor proteins and targets of thiosemicarbazones. J. Biol. Chem. 301, 110230.

Bas-Orth, C., et al., 2017. Synaptic activity drives a genomic program that promotes a neuronal Warburg effect. J. Biol. Chem. 292, 5183–5194.

Beaulieu, J.M., 2012. A role for Akt and glycogen synthase kinase-3 as integrators of dopamine and serotonin neurotransmission in mental health. J. Psychiatry Neurosci. 37, 7–16.

Bednarek, E., Caroni, P., 2011. B-Adducin is required for stable assembly of new synapses and improved memory upon environmental enrichment. Neuron 69, 1132–1146.

Ben Zablah, Y., et al., 2020. The role of ADF/Cofilin in synaptic physiology and Alzheimer's disease. Front. Cell Dev. Biol. 8, 594998.

Benarroch, E., 2024. What is the role of lactate in brain metabolism, plasticity, and neurodegeneration? Neurology 102, e209378.

Biggi, S., et al., 2017. Evidence of presynaptic localization and function of the c-Jun N-terminal kinase. Neural Plast. 2017, 6468356.

Björkblom, B., et al., 2005. Constitutively active cytoplasmic c-Jun N-terminal kinase 1 is a dominant regulator of dendritic architecture: role of microtubule-associated protein 2 as an effector. J. Neurosci. 25, 6350–6361.

Borsello, T., Bonny, C., 2004. Use of cell-permeable peptides to prevent neuronal degeneration. Trends Mol. Med. 10, 239–244.

Borsello, T., et al., 2003. A peptide inhibitor of c-Jun N-terminal kinase protects against excitotoxicity and cerebral ischemia. Nat. Med. 9, 1180–1186.

Bouzier-Sore, A.K., et al., 2006. Competition between glucose and lactate as oxidative energy substrates in both neurons and astrocytes: a comparative NMR study. Eur. J. Neurosci. 24, 1687–1694.

Castro-Torres, R.D., et al., 2021. Dual. Int. J. Mol. Sci. 22.

Chakraborti, S., et al., 2016. The emerging role of the tubulin code: from the tubulin molecule to neuronal function and disease. Cytoskeleton (Hoboken). 73, 521–550.

Chang, L., et al., 2003. JNK1 is required for maintenance of neuronal microtubules and controls phosphorylation of microtubule-associated proteins. Dev. Cell 4, 521–533.

Chew, L.A., Khanna, R., 2018. CRMP2 and voltage-gated ion channels: potential roles in neuropathic pain. Neuron. Sign. 2.

Coffey, E.T., 2014. Nuclear and cytosolic JNK signalling in neurons. Nat. Rev. Neurosci. 15, 285–299.

Coffey, E.T., et al., 2000. Dual roles for c-Jun N-terminal kinase in developmental and stress responses in cerebellar granule neurons. J. Neurosci. 20, 7602–7613.

Coffey, E.T., et al., 2002. C-Jun N-terminal protein kinase (JNK) 2/3 is specifically activated by stress, mediating c-Jun activation, in the presence of constitutive JNK1 activity in cerebellar neurons. J. Neurosci. 22, 4335–4345.

Cole, A.R., et al., 2004. GSK-3 phosphorylation of the Alzheimer epitope within collapsin response mediator proteins regulates axon elongation in primary neurons. J. Biol. Chem. 279, 50176–50180.

Cole, A.R., et al., 2006. Distinct priming kinases contribute to differential regulation of collapsin response mediator proteins by glycogen synthase kinase-3 in vivo. J. Biol. Chem. 281, 16591–16598.

Crofton, E.J., et al., 2017. Glycogen synthase kinase 3 beta alters anxiety-, depression-, and addiction-related behaviors and neuronal activity in the nucleus accumbens shell. Neuropharmacology 117, 49–60.

Cruz, J.C., et al., 2003. Aberrant Cdk5 activation by p25 triggers pathological events leading to neurodegeneration and neurofibrillary tangles. Neuron 40, 471–483.

Dent, E.W., 2020. Dynamic microtubules at the synapse. Curr. Opin. Neurobiol. 63, 9–14.

Duncan, B.W., et al., 2021. Molecular mechanisms of L1 and NCAM adhesion molecules in synaptic pruning, plasticity, and stabilization. Front. Cell Dev. Biol. 9, 625340.

Elo, L.L., et al., 2009. Optimized detection of differential expression in global profiling experiments: case studies in clinical transcriptomic and quantitative proteomic datasets. Brief. Bioinform. 10, 547–555.

Fiol, C.J., et al., 1987. Formation of protein kinase recognition sites by covalent modification of the substrate. Molecular mechanism for the synergistic action of casein kinase II and glycogen synthase kinase 3. J. Biol. Chem. 262, 14042–14048.

Fu, M.M., Holzbaur, E.L., 2013. JIP1 regulates the directionality of APP axonal transport by coordinating kinesin and dynein motors. J. Cell Biol. 202, 495–508.

Gehringer, M., et al., 2015. c-Jun N-terminal kinase inhibitors: a patent review (2010–2014). Expert Opin. Ther. Pat. 25, 849–872.

Gould, T.D., et al., 2004. In vivo evidence in the brain for lithium inhibition of glycogen synthase kinase-3. Neuropsychopharmacology 29, 32–38.

Grubisha, M.J., et al., 2022. Trio and Kalirin as unique enactors of Rho/Rac spatiotemporal precision. Cell. Signal. 98, 110416.

Gu, J., et al., 2010. ADF/cofilin-mediated actin dynamics regulate AMPA receptor trafficking during synaptic plasticity. Nat. Neurosci. 13, 1208–1215.

Gu, Z., et al., 2014. Circlize implements and enhances circular visualization in R. Bioinformatics 30, 2811–2812.

Hirosumi, J., et al., 2002. A central role for JNK in obesity and insulin resistance. Nature 420, 333–336.

Hollos, P., et al., 2018. JNK regulation of depression and anxiety. Brain Plast. 3, 145–155.

Hollos, P., et al., 2020. Optogenetic control of spine-head JNK reveals a role in dendritic spine regression. eNeuro 7.

Hong, Y., et al., 2022. PhosPiR: an automated phosphoproteomic pipeline in R. Brief. Bioinform. 23.

Hong, Y., et al., 2024. Jnk1 and downstream signalling hubs regulate anxiety-like behaviours in a zebrafish larvae phenotypic screen. Sci. Rep. 14, 11174.

Hotamisligil, G.S., Davis, R.J., 2016. Cell signaling and stress responses. Cold Spring Harb. Perspect. Biol. 8.

Hsu, H.J., et al., 2010. Stretch-induced stress fiber remodeling and the activations of JNK and ERK depend on mechanical strain rate, but not FAK. PLoS One 5, e12470.

Iordanov, M.S., et al., 1997. Ribotoxic stress response: activation of the stress-activated protein kinase JNK1 by inhibitors of the peptidyl transferase reaction and by sequence-specific RNA damage to the alpha-sarcin/ricin loop in the 28S rRNA. Mol. Cell. Biol. 17, 3373–3381.

Jahn, R., et al., 2024. Mechanisms of SNARE proteins in membrane fusion. Nat. Rev. Mol. Cell Biol. 25, 101–118.

Karbe, Y., et al., 2013. Phosphorylation of serine 774 of the neural cell adhesion molecule (NCAM) is involved in the interaction with collapsin response mediator protein-2. Neurochem. Res. 38, 1229–1235.

Karlsson, M., et al., 2021. A single-cell type transcriptomics map of human tissues. Sci. Adv. 7.

Karpac, J., et al., 2009. JNK signaling in insulin-producing cells is required for adaptive responses to stress in Drosophila. Aging Cell 8, 288–295.

Komulainen, E., et al., 2014. JNK1 controls dendritic field size in L2/3 and L5 of the motor cortex, constrains soma size, and influences fine motor coordination. Front. Cell. Neurosci. 8, 272.

Komulainen, E., et al., 2020. Impact of JNK and its substrates on dendritic spine morphology. Cells 9.

Kumari, S., et al., 2023. Apoptosis in Alzheimer's disease: insight into the signaling pathways and therapeutic avenues. Apoptosis 28, 943–957.

Kurokawa, M., et al., 2008. Inhibition of apoptosome formation by suppression of Hsp90beta phosphorylation in tyrosine kinase-induced leukemias. Mol. Cell. Biol. 28, 5494–5506.

Kyriakis, J.M., Avruch, J., 2012. Mammalian MAPK signal transduction pathways activated by stress and inflammation: a 10-year update. Physiol. Rev. 92, 689–737.

Levina, A., et al., 2022. Activation of the essential kinase PDK1 by phosphoinositide-driven trans-autophosphorylation. Nat. Commun. 13, 1874.

Li, X., Jope, R.S., 2010. Is glycogen synthase kinase-3 a central modulator in mood regulation? Neuropsychopharmacology 35, 2143–2154.

Liu, F., et al., 2004. O-GlcNAcylation regulates phosphorylation of tau: a mechanism involved in Alzheimer's disease. Proc. Natl. Acad. Sci. USA 101, 10804–10809.

Maheras, K.J., et al., 2018. Absence of Claudin 11 in CNS myelin perturbs behavior and neurotransmitter levels in mice. Sci. Rep. 8, 3798.

Marchisella, F., et al., 2016. Microtubule and microtubule associated protein anomalies in psychiatric disease. Cytoskeleton (Hoboken) 10, 596–611.

Mines, M.A., et al., 2010. GSK3 influences social preference and anxiety-related behaviors during social interaction in a mouse model of fragile X syndrome and autism. PLoS One 5, e9706.

Mizuno, K., 2013. Signaling mechanisms and functional roles of cofilin phosphorylation and dephosphorylation. Cell. Signal. 25, 457–469.

Mohammad, H., et al., 2018. JNK1 controls adult hippocampal neurogenesis and imposes cell-autonomous control of anxiety behaviour from the neurogenic niche. Mol. Psychiatry 23, 362–374.

Morfini, G.A., et al., 2009. Pathogenic huntingtin inhibits fast axonal transport by activating JNK3 and phosphorylating kinesin. Nat. Neurosci. 12, 864–871.

Mori, Y., et al., 2008. JNK phosphorylates synaptotagmin-4 and enhances Ca2+−evoked release. EMBO J. 27, 76–87.

Murray, J.T., et al., 2004. Exploitation of KESTREL to identify NDRG family members as physiological substrates for SGK1 and GSK3. Biochem. J. 384, 477–488.

Olszowy, P.P., Burns, A., Ciborowski, P.S., 2013. Pressure-assisted sample preparation for proteomic analysis. Anal Biochem. 438 (1), 67–72. https://doi.org/10.1016/j.ab.2013.03.023. PMID: 23545193. ; PMCID: PMC3761939. Epub 2013 Mar 29.

Peng, J., Andersen, J.K., 2003. The role of c-Jun N-terminal kinase (JNK) in Parkinson's disease. IUBMB Life 55, 267–271.

Pereira, A.M., et al., 2011. Integrin-dependent activation of the JNK signaling pathway by mechanical stress. PLoS One 6, e26182.

Pielage, J., et al., 2011. Hts/Adducin controls synaptic elaboration and elimination. Neuron 69, 1114–1131.

Pratt, M.R., Vocadlo, D.J., 2023. Understanding and exploiting the roles of O-GlcNAc in neurodegenerative diseases. J. Biol. Chem. 299, 105411.

Repici, M., Borsello, T., 2006. JNK pathway as therapeutic target to prevent degeneration in the central nervous system. Adv. Exp. Med. Biol. 588, 145–155.

Rickman, C., Duncan, R.R., 2010. Munc18/Syntaxin interaction kinetics control secretory vesicle dynamics. J. Biol. Chem. 285, 3965–3972.

Rui, Y., et al., 2007. A beta-catenin-independent dorsalization pathway activated by Axin/JNK signaling and antagonized by aida. Dev. Cell 13, 268–282.

Sayas, C.L., Ávila, J., 2021. GSK-3 and tau: a key duet in Alzheimer's disease. Cells 10.

Scales, T.M., et al., 2009. Nonprimed and DYRK1A-primed GSK3 beta-phosphorylation sites on MAP1B regulate microtubule dynamics in growing axons. J. Cell Sci. 122, 2424–2435.

Seifert, F., et al., 2007. Phosphorylation of serine 264 impedes active site accessibility in the E1 component of the human pyruvate dehydrogenase multienzyme complex. Biochemistry 46, 6277–6287.

Shekar, A., et al., 2023. Syntaxin 1 Ser. Sci. Adv. 9, eadd8417.

Shi, V.H., et al., 2021. Phosphorylation of Syntaxin-1a by casein kinase 2α regulates presynaptic vesicle exocytosis from the reserve pool. J. Neurochem. 156, 614–623.
Shimada, T., et al., 2024. Neuritin controls axonal branching in serotonin neurons: a possible mediator involved in the regulation of depressive and anxiety behaviors via FGF signaling. J. Neurosci. 44.
Shinde, M.Y., et al., 2017. Phosphoproteomics reveals that glycogen synthase kinase-3 phosphorylates multiple splicing factors and is associated with alternative splicing. J. Biol. Chem. 292, 18240–18255.
Solas, M., et al., 2023. JNK activation in Alzheimer's disease is driven by amyloid β and is associated with tau pathology. ACS Chem. Neurosci. 14, 1524–1534.
Solinas, G., Becattini, B., 2017. JNK at the crossroad of obesity, insulin resistance, and cell stress response. Mol. Metab. 6, 174–184.
Stambolic, V., et al., 1996. Lithium inhibits glycogen synthase kinase-3 activity and mimics wingless signalling in intact cells. Curr. Biol. 6, 1664–1668.
Stratton, H., et al., 2020. Coordinating synaptic signaling with CRMP2. Int. J. Biochem. Cell Biol. 124, 105759.
Teng, J., et al., 2001. Synergistic effects of MAP2 and MAP1B knockout in neuronal migration, dendritic outgrowth, and microtubule organization. J. Cell Biol. 155, 65–76.
Thomas, G.M., et al., 2008. Rapid and bi-directional regulation of AMPA receptor phosphorylation and trafficking by JNK. EMBO J. 27, 361–372.
Trivedi, N., et al., 2005. Glycogen synthase kinase-3beta phosphorylation of MAP1B at Ser1260 and Thr1265 is spatially restricted to growing axons. J. Cell Sci. 118, 993–1005.
Uchida, Y., et al., 2019. Involvement of Claudin-11 in disruption of blood-brain, -spinal cord, and -arachnoid barriers in multiple sclerosis. Mol. Neurobiol. 56, 2039–2056.
van Hall, G., et al., 2009. Blood lactate is an important energy source for the human brain. J. Cereb. Blood Flow Metab. 29, 1121–1129.
Vind, A.C., et al., 2024. Death by ribosome. Trends Cell Biol. 7, 615–626.
Wang, D., et al., 2015. F-actin binding protein, anillin, regulates integrity of intercellular junctions in human epithelial cells. Cell. Mol. Life Sci. 72, 3185–3200.
Wyss, M.T., et al., 2011. In vivo evidence for lactate as a neuronal energy source. J. Neurosci. 31, 7477–7485.
Xu, P., et al., 2011. JNK regulates FoxO-dependent autophagy in neurons. Genes Dev. 25, 310–322.
Yang, X., et al., 2023. Functional regulation of syntaxin-1: an underlying mechanism mediating exocytosis in neuroendocrine cells. Front. Endocrinol. (Lausanne) 14, 1096365.
Yao, S., et al., 2023. Astrocytic lactate dehydrogenase a regulates neuronal excitability and depressive-like behaviors through lactate homeostasis in mice. Nat. Commun. 14, 729.
Zeng, C., et al., 2022. JNK initiates Beclin-1 dependent autophagic cell death against Akt activation. Exp. Cell Res. 414, 113105.
Zhang, J., et al., 1994. Phosphorylation of Thr642 is an early event in the processing of newly synthesized protein kinase C beta 1 and is essential for its activation. J. Biol. Chem. 269, 19578–19584.
Zhao, H.B., et al., 2017. Xiao Yao san improves the anxiety-like behaviors of rats induced by chronic immobilization stress: the involvement of the JNK signaling pathway in the Hippocampus. Biol. Pharm. Bull. 40, 187–194.
Zhou, X., et al., 2023. Stress-activated protein kinase JNK modulates depression-like behaviors in mice. Mol. Neurobiol. 60, 2367–2378.
Ziak, J., et al., 2020. CRMP2 mediates Sema3F-dependent axon pruning and dendritic spine remodeling. EMBO Rep. 21, e48512.
Ziak, J., et al., 2024. Microtubule-binding protein MAP1B regulates interstitial axon branching of cortical neurons via the tubulin tyrosination cycle. EMBO J. 43, 1214–1243.